Alexandria Engineering Journal (2015) 54, 429–446

Alexandria University

Alexandria Engineering Journal

www.elsevier.com/locate/aej
www.sciencedirect.com

ORIGINAL ARTICLE

ANN and RSM approach for modeling and optimization of designing parameters for a V down perforated baffle roughened rectangular channel

Sunil Chamoli *

Department of Mechanical Engineering, DIT University, Dehradun, Uttarakhand 248001, India

Received 5 September 2014; revised 26 March 2015; accepted 31 March 2015
Available online 24 April 2015

KEYWORDS

Perforated baffles;
Nusselt number;
Friction factor;
RSM;
ANN

Abstract The turbulence promoters are widely used to enhance the performance of rectangular channel which were used for turbine blade passage cooling. In the present study, the influence of design parameters of the V down perforated baffle roughened rectangular channel on the heat transfer and friction factor was investigated using RSM and ANN. The quadratic model generated by RSM is used to predict the performance parameters, i.e. Nusselt number and friction factor with reasonably good accuracy. The optimum values of the design parameters of the V down perforated baffle roughened rectangular channel are relative roughness pitch of 2.6, relative roughness height of 0.33, open area ratio of 18% and Reynolds number of 18,500, in the desirable range of the order of 0.95. The training of the experimental data is carried out using 4-10-2 neural network and the predicted values are compared with the experimental values and found deviation in the range of ±10% among predicted and experimental values. The comparison of predicted values by RSM and ANN with the experimental values was carried out for each run of experiment and it was observed that the RSM predicted values are in accord with the experimental values in the uncertainty range of ±5%.

1. Introduction

In thermal processes, heat transfer is one of the most important topics to draw the attention of related researchers and scientists. The most effective way of heat transfer enhancement in a rectangular channel was using the vortex generators and rib turbulators as roughness elements. Numerous studies have been carried out for studying the heat transfer and friction factor characteristics of roughened rectangular channel both experimentally and numerically [1–19]. The solid baffles vortex generators enhanced the heat transfer rate and it is also accompanied with a high friction penalty. The perforated baffles as roughness element are found more suitable turbulence promoters than solid ones for enhancing the thermohydraulic performance of rectangular channel [12–14]. The most of the studies in this field have intensified on the heat transfer enhancement. On the reverse, the optimization of the heat transfer devices is a topic that just being area of research of the investigators working in the field of heat transfer enhancement. Several heat

* Tel.: +91 9897870171.
E-mail address: mech.chamoli@gmail.com
Peer review under responsibility of Faculty of Engineering, Alexandria University.

http://dx.doi.org/10.1016/j.aej.2015.03.018

Nomenclature

ANN	artificial neural network
CCD	central composite design
e/H	relative roughness height
f	friction factor
Nu	Nusselt number
P/e	relative roughness pitch
Re	Reynolds number
$x_1, x_2 \ldots x_n$	independent input variables
y	desired response
β	open area ratio
ε	fitting error

transfer enhancement elements have been brought out to improve the thermal and thermohydraulic performance of rectangular duct. The issue of different design parameters of the roughness elements on the Nusselt number and friction characteristics has been investigated by numerous investigators. Few of the examples are, rectangular channel duct fitted with ribs [1–5,7–9], delta winglets [17,19] and baffles [6,10,11,13,14,20,21].

The response surface methodology (RSM) is an empirical modeling approach for defining the relationship between various process parameters and responses with the various desired criteria and searching the significance of these process parameters on the coupled responses. It is a sequential experimentation strategy for ramping up and optimizing the empirical model. Response surface methodology (RSM) uses various statistical, graphical, and mathematical techniques to acquire, improve, or optimize a process. Therefore RSM has been frequently used in optimizing the flow and geometrical parameters of roughened rectangular channel in thermal process systems [23].

Ref. [22] investigated the parameter optimization of a pin fin type heat sink using response surface methodology and the parametric study identified the important influence factors to minimize thermal resistance and pressure drop. Ref. [23] used RSM for modeling and optimization of designing parameters for a parallel plain fin heat sink with confined jet. The optimum designing parameters of PPF heat sink with an axial-flow cooling fan under the constrains of mass and space limitation, which are based on the quadratic model of RSM and the sequential approximation optimization method, are found to be fin height of 60 mm, fin thickness of 1.07 mm, passage width between fins of 3.32 mm, and the distance between the cooling fan and the type of fins of 2.03 mm. Multi-objective optimization of outward convex corrugated tubes using response surface methodology was carried out by Ref. [24]. Response surface analysis was utilized by Ref. [25] to evaluate the axis ratio effect on the overall thermohydraulic performance of the elliptical finned tube heat exchanger. It was found that the increase of the axis ratio improves the overall thermohydraulic performance at higher air velocity or lower water volumetric flow rate, but the opposite effect is observed at a lower air velocity or higher water volumetric flow rate. Ref. [26] investigated the thermal performance of the S shaped elements by response surface methodology. The element height, the transverse pitch, the element radius, and the Reynolds number were taken as variables to analyze the thermal performance in terms of the Nusselt number and the friction factor and the results show that the RSM is an efficient technique to forecast the operation of such arrangements. Thermal and thermohydraulic performance of double pass packed solar air heater under external recycle was carried out by Ref. [27], using analytical and RSM combined approach. The study discovered that the RSM proposed mathematical model is in full accord with the observational outcomes. In the last two decades, the use of artificial intelligence methods in mechanical engineering is increasing bit by bit. This is primarily because of the effectiveness of artificial intelligence modeling systems having improved in a large deal in the engineering field. Artificial neural networks by employing a great number of parameters (weights and biases) are capable to estimate target data of thermal systems in engineering applications with a high accuracy. Ref. [28] used ANN to correlate experimentally determined Colburn j-factors and Fanning friction factors for flow of fluid water in square tubes with internal helical fins. ANNs trained with the combined database showed satisfactory results, and were superior to algebraic power-law correlations developed by the merged database. ANN approach successfully was employed in predicting the heat transfer and fluid flow characteristics of roughened heat exchangers, in addition to the thermal and thermohydraulic performance of solar thermal systems with reasonably good accuracy with the experimental results [29–33]. The literature study revealed that the perforated baffle roughened rectangular channel significantly enhanced the heat transfer rate over the smooth channel. It has been set up that the RSM and ANN techniques were successfully used to anticipate the performance of roughened channel and heat exchangers with a relatively higher level of accuracy with experimental results. The present work was carried out with an aim to anticipate the operation of the V down perforated baffle roughened rectangular channel with RSM and ANN approaches. The anticipated outcomes are likewise taken to compare with the experimental observations to ascertain the accurate data prediction with RSM and ANN approaches. Ultimately the objective was to find the optimum roughness parameter that yields maximum performance of the V down perforated baffle roughened rectangular channel.

2. Experimental work

Fig. 1 illustrates a schematic diagram of the experimental setup. The principal characteristics of the observational detail and data reduction are given elsewhere [14]. The experimental apparatus mainly consists of inlet, test and outlet section of 700, 1300 and 400 mm length, respectively. The rectangular channel duct has an aspect ratio of 10, with a width of 350 mm and height of 35 mm. The elements of the experimental setup are a blower, wooden rectangular duct, electric heater, GI pipe, control valves, orifice plate, U tube manometer,

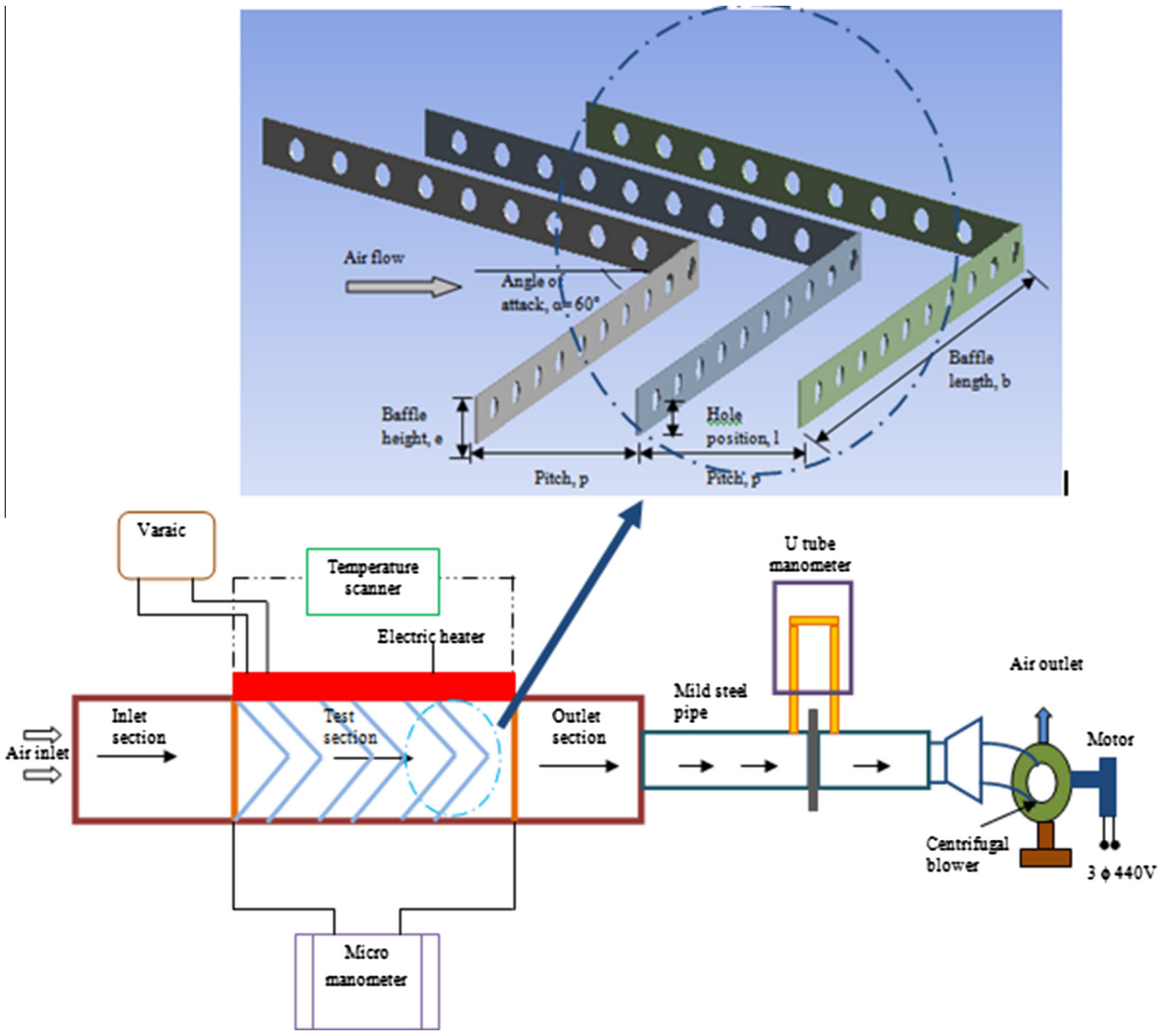

Figure 1 Schematic diagram of the experimental test rig [14].

micromanometer, variable transformer, thermocouples and temperature scanner as shown in Fig. 1. An electric heater having size of 1300 mm × 350 mm is fabricated by combining series and parallel loops of heating wire on a thick asbestos sheet of 5 mm thickness. A mica sheet of 1 mm thickness was identified over the electric heater wire to deliver a uniform heat flux over the test plate. The heat flux of intensity 1000 W/m^2 is provided over the test plate with the help of variable transformer. The T type copper constantan thermocouples were used to evaluate the test plate, inlet and outlet temperatures. The volume flow rate of air is measured by means of calibrated orifice meter attached to a U tube manometer. The control valves were provided to alter the flow Reynolds number. A temperature scanner was employed to measure the temperatures and pressure drop across the test section was evaluated with the aid of a digital micromanometer. The roughened test plates are made up with 0.9 mm thick GI sheet. The V down perforated baffle turbulators were used as a roughness element with different configurations, viz. relative roughness pitch (P/e), relative roughness height (e/H) and open area ratio (β).

3. Response surface methodology

RSM is a widely accepted statistical technique used for experimental purpose. RSM approach proceeds with carrying out statistically designed experiments, followed by evaluating the coefficients in a mathematical model and the prediction of response and examining the sufficiency of the model. It is very useful for modeling and predicting the reaction of interest affected by a number of input variables with the aim of optimizing the responses. In the RSM, the quantitative pattern of relationship between desired response and independent input variables can be interpreted equally. RSM can find the optimal set of experimental parameters that bring forth a maximum or minimum value of response, and can represent the direct and interactive effects of process parameters through two and three-dimensional plots. In the RSM, the quantitative pattern of relationship between desired response and independent input variables could be interpreted as

$$y = f(x_1, x_2, x_3 \ldots\ldots x_n) \pm \varepsilon \quad (1)$$

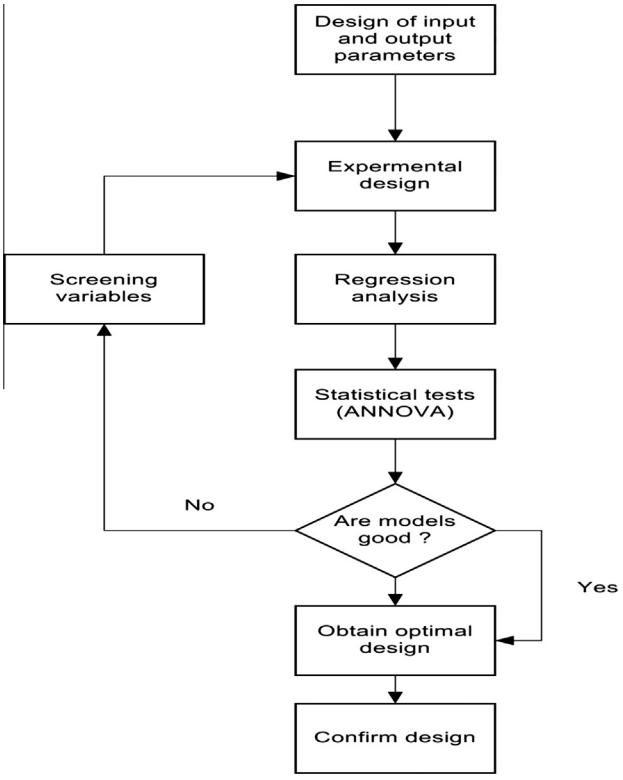

Figure 2 Flowchart of the RSM modeling approach for optimal design.

where y is the response of the system, while x_n is the variables called factors and ε is the fitting error.

The appearance of the response function is a surface as plotting the expected response of f. The recognition of suitable approximation of f will determine whether the application of RSM is successful or not. The necessary data for constructing the response models are mostly collected by the design of experiments. In this study, the collection of experimental data adopts the face centered CCD and the approximation will be proposed using the fitted second-order polynomial regression model which is called the quadratic model. The quadratic model of f can be written as follows:

$$f = a_o + \sum_{i=1}^{n} a_i x_i + \sum_{i=1}^{n} a_{ii} x_i + \sum_{i<j}^{n} a_{ij} x_i x_j + \varepsilon \quad (2)$$

where a_i represents the linear effect of x_i, a_{ii} represents the quadratic effect of x_i and a_{ij} represents the linear-linear interactions between x_i and x_j, then response surface contains the linear, square and cross product terms. The response surface method is a sequential process and its procedure can be summarized as shown in Fig. 2.

4. Experimental conditions and plan

The standard RSM is based on three types of design of experiments (DOE) matrices, including central composite designs (CCD), Box Behnken design (BBD) and expected integrated mean squared error optimal (EIMSE-optimal). The most popular response surface method (RSM) design is the central composite design (CCD), shown in Fig. 3. In this study, three-factor CCD model is used. The flow and geometrical parameters that strongly affect the thermal and the thermohydraulic performance of the V down perforated baffle roughened rectangular channel are used in the study, viz. relative roughness pitch (P/e), relative roughness height (e/H), open area ratio (β) and flow Reynolds number (Re). These parameters are used as design variables of the V down perforated baffle roughened rectangular channel. The factors and their levels are given in Table 1. In this investigation, total 30 experiments were conducted at the stipulated conditions based on the face centered CCD. The response variables investigated are the Nusselt number (Nu) and the friction factor (f). The data obtained from experimental studies were analyzed using the software program so-called Design Expert 9.0.3.

5. ANN model for performance prediction

ANNs consisting of very simple and highly interconnected processors called neuron are a computational structure

Table 1 Factors and levels of the experimental design.

S/no.	Factors	Level		
		−1	0	+1
1	P/e	1	2	3
2	e/H	0.285	0.4	0.514
3	β	12	24	36
4	Re	4100	12,000	18,500

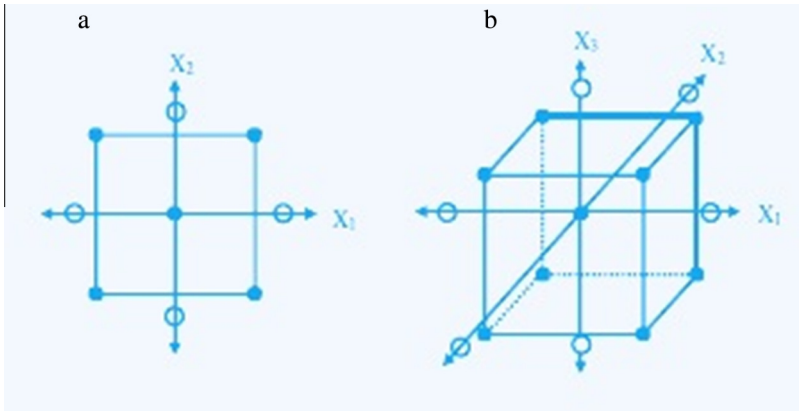

Figure 3 (a) Two factor central composite design model and (b) three factor central composite design model.

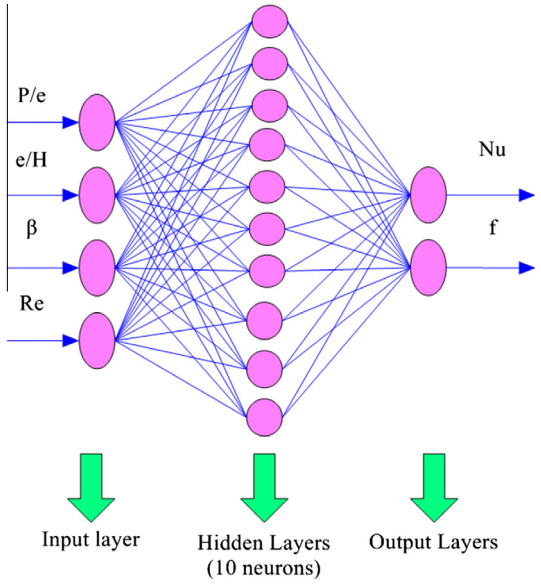

Figure 4a Feed-forward neural network (the ANN has one hidden layer with ten hidden neurons and one output layer with two outputs, briefly written as 4-10-2.

inspired by biological neural systems. The processors are analogous to biological neurons in the human head. The neurons are related to each other by weighted links over which signals can go. Each neuron receives multiple inputs from other neurons in proportion to their connection weights and gets a single end product which may be distributed to several other nerve cells [34].

Feed forward with backward propagation is one of the most common neural networks used in solving the engineering problems. In this, there exists a mathematically strict learning scheme to train the network and guarantee mapping between inputs and outputs. In the present study the neural network architecture used is shown in Fig. 4a. This form takes in one input layer, one hidden layer and one output layer. The number of neurons in the input and output layers is equal to the input and output variables, respectively. Yet, in the hidden layer different numbers of neurons can be employed and it is significant for optimization of the network mesh. At the present network total number of 10 neurons in hidden layers is selected and is shown in Fig. 4b.

The input layer contains 4 neurons having one neuron each for parametric inputs, viz. e/H, P/e, β and Re, respectively. The hidden layers contain 10 neurons while the output layer contains two neurons having output Nu and f. As far as in

Table 2 Design of experimental matrix and results of the V down perforated baffle rectangular channel performance characteristics.

Run no.	Design parameters				Experimental results	
	P/e	e/H	β	Re	Nu	f
1	−1	1	1	−1	34.78	0.0797
2	0	0	0	0	89.69	0.0425
3	1	−1	−1	−1	34.70	0.0444
4	0	0	0	0	89.69	0.0425
5	1	0	0	0	89.69	0.0425
6	1	1	1	−1	35.64	0.0698
7	−1	1	−1	−1	37.12	0.0911
8	−1	1	−1	1	122.67	0.0683
9	1	−1	1	−1	32.51	0.0411
10	−1	−1	−1	1	114.11	0.0414
11	−1	−1	−1	−1	35.00	0.0550
12	0	−1	0	0	84.32	0.0353
13	−1	−1	1	1	96.65	0.0342
14	0	0	0	1	129.73	0.0391
15	0	0	0	0	89.69	0.0425
16	0	0	0	0	89.69	0.0425
17	0	0	0	−1	37.40	0.0503
18	0	0	0	0	89.69	0.0425
19	−1	−1	1	−1	31.62	0.0484
20	1	1	1	1	117.77	0.0517
21	1	−1	−1	1	114.84	0.0316
22	0	1	0	0	96.06	0.0620
23	0	0	1	0	87.21	0.0413
24	1	1	−1	1	129.73	0.0575
25	1	1	−1	−1	37.95	0.0787
26	−1	1	1	1	111.31	0.0613
27	0	0	0	0	89.69	0.0425
28	0	0	−1	0	89.69	0.0425
29	−1	0	0	0	82.43	0.0464
30	1	−1	1	1	108.22	0.0304

the training procedure of the neural networks, the input and output data had several physical units and range sizes, and all data were normalized in the 0–1 range to avoid any computational difficulty using the following relation:

$$\text{Normalized data} = (\text{data value} - \text{minimum value})/(\text{maximum value} - \text{minimum value}) \quad (3)$$

The Levenberg–Marquardt back propagation algorithm was used for the preparation of the ANNs. In this method, weights and biases iteratively adjust to reduce diversion of the predicted values of the net from the desired values according to the Levenberg–Marquardt [35–37] optimization procedure. In parliamentary law to assess the robustness of the

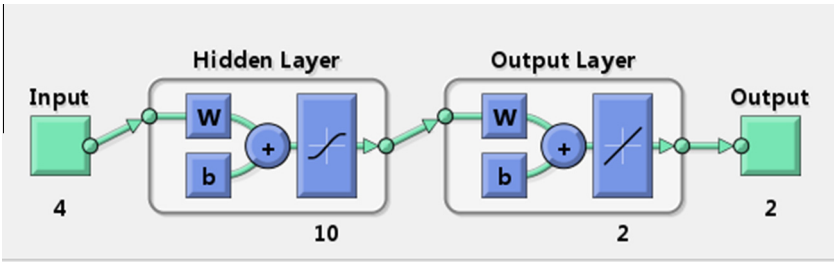

Figure 4b Feed-forward with the backward propagation neural network used in the present study.

Table 3 ANOVA table for the Nusselt number (before elimination).

Source	Sum of squares	DF	Mean square	*f*-Value	Prob > *F*	
Model	31663.3404	14	2261.667	273.0336	< 1.95E−15	Significant
A	68.2627	1	68.26272	8.24083	0.011668	
B	277.0039	1	277.0039	33.44054	< 3.61E−05	
C	197.7214	1	197.7214	23.86938	< 0.000198	
D	29466.1191	1	29466.12	3557.217	< 3.03E−19	
AB	0.3419	1	0.341908	0.041276	0.841737	
AC	8.2004	1	8.200416	0.989973	0.33553	
AD	35.5413	1	35.54127	4.290622	0.055984	
BC	0.1800	1	0.179972	0.021727	0.88478	
BD	82.8074	1	82.80743	9.9967	0.006449	
CD	84.3992	1	84.3992	10.18886	0.006062	
A^2	62.2316	1	62.23157	7.512736	0.01516	
B^2	1.4679	1	1.467857	0.177203	0.679757	
C^2	16.3801	1	16.38006	1.977438	0.180038	
D^2	30.9862	1	30.98622	3.740726	0.072196	
Residual	124.2521	15	8.283476			
Lack of fit	124.2521	10	12.42521			
Pure error	0.0000	5	0			
Cor total	31787.5925	29				
Std. Dev.	2.8781		R-Squared	0.996091		
Mean	80.9763		Adj R-Squared	0.992443		
C.V. (%)	3.5543		Pred R-Squared	0.980638		
PRESS	615.4712		Adeq Precision	48.78826		

Table 4 ANOVA table for the Nusselt number (after backward elimination).

Source	Sum of squares	DF	Mean square	*f*- Value	Prob > *F*	
Model	31653.1502	10	3165.315	447.3368	2.35E−20	Significant
A	68.2677	1	68.2677	9.647904	0.005815	
B	277.0714	1	277.0714	39.157	5.22E−06	
C	197.7154	1	197.7154	27.94204	4.21E−05	
D	29466.1191	1	29466.12	4164.287	1E−23	
AD	35.5416	1	35.54159	5.022901	0.037153	
BD	82.8097	1	82.80972	11.70305	0.002865	
CD	84.3988	1	84.39884	11.92763	0.002661	
A^2	74.5117	1	74.51171	10.53034	0.004261	
C^2	21.2617	1	21.26167	3.004796	0.099217	
D^2	38.4484	1	38.44835	5.433697	0.030918	
Residual	134.4423	19	7.07591			
Lack of fit	134.4423	14	9.603021			
Pure error	0.0000	5	0			
Cor total	31787.5925	29				
Std. Dev.	2.6601		R-Squared	0.995771		
Mean	80.9763		Adj R-Squared	0.993545		
C.V. (%)	3.2850		Pred R-Squared	0.986715		
PRESS	422.3093		Adeq Precision	61.64305		

model, all input data points were separated into two sections: the train and test data set, 60% of the data points were selected for training to develop the neural network and the remaining data were considered as the test data set and validation in the proportion of 20% each. Moreover, trial-and-error method was used to determine the appropriate number of neurons in the hidden layer.

6. Results and discussion

In this study the different values of geometrical parameters were required on account of their effect on Nusselt number and friction factor. The total number of 30 runs of experiments was taken on the basis of CCD RSM methodology and the same runs of experimental data were trained in ANN.

On the basis of three factor three level face centered CCD, a design matrix has been formed. The design matrix and the simulated analytical results of the different response variables are presented in Table 2. In parliamentary law to examine the fit of the quadratic model with the observational data obtained in this study, the test for significance of the regression model and the test for significance of individual model coefficients are performed. The analysis of variance (ANOVA) is used to summarize the above tests performed.

Table 5 ANOVA table for the friction factor (before elimination).

Source	Sum of squares	DF	Mean square	*f*- Value	Prob > F	
Model	0.0065	14	0.000462	148.4275	< 1.81E−13	Significant
A	0.0003	1	0.000337	108.3002	< 2.95E−08	
B	0.0037	1	0.003715	1194.276	< 1.03E−15	
C	0.0002	1	0.000154	49.38706	< 4.09E−06	
D	0.0011	1	0.001136	365.3002	< 6.08E−12	
AB	0.0000	1	7.65E−06	2.459965	0.137632	
AC	0.0000	1	1.03E−05	3.317309	0.088556	
AD	0.0000	1	2.61E−06	0.838223	0.37439	
BC	0.0000	1	1.35E−05	4.354482	0.054394	
BD	0.0001	1	5.37E−05	17.27375	0.000845	
CD	0.0000	1	5.65E−06	1.816452	0.197741	
A^2	0.0000	1	2.04E−05	6.55067	0.021787	
B^2	0.0001	1	0.00013	41.65129	< 1.09E−05	
C^2	0.0000	1	2.15E−07	0.068952	0.796441	
D^2	0.0000	1	1.4E−05	4.49565	0.051065	
Residual	0.0000	15	3.11E−06			
Lack of fit	0.0000	10	4.67E−06			
Pure error	0.0000	5	0			
Cor total	0.0065	29				
Std. Dev.	0.0018		R-Squared	0.992833		
Mean	0.0500		Adj R-Squared	0.986144		
C.V. (%)	3.5303		Pred R-Squared	0.965966		
PRESS	0.0002		Adeq Precision	47.40591		

Table 6 ANOVA table for the friction factor (after backward elimination).

Source	Sum of squares	DF	Mean square	*f*-Value	Prob > *F*	
Model	0.0064	10	0.000645	195.1263	< 5.81E−17	Significant
A	0.0003	1	0.000336	101.7738	< 4.57E−09	
B	0.0037	1	0.003715	1124.25	< 2.27E−18	
C	0.0002	1	0.000153	46.29334	< 1.7E−06	
D	0.0011	1	0.001136	343.8808	< 1.25E−13	
AC	0.0000	1	1.03E−05	3.122798	0.093263	
BC	0.0000	1	1.35E−05	4.098907	0.057198	
BD	0.0001	1	5.37E−05	16.2608	0.000711	
A^2	0.0000	1	2.37E−05	7.172169	0.014875	
B^2	0.0001	1	0.000145	43.99816	< 2.4E−06	
D^2	0.0000	1	1.65E−05	4.981459	0.037858	
Residual	0.0001	19	3.3E−06			
Lack of fit	0.0001	14	4.49E−06			
Pure error	0.0000	5	0			
Cor total	0.0065	29				
Std. Dev.	0.0018		R-Squared	0.990357		
Mean	0.0500		Adj R-Squared	0.985281		

6.1. ANOVA

F test analysis of variance (ANOVA) is performed and presented in Table 3, to check the statistical significance of the quadratic model for Nusselt number. Values of "Prob > *F*" in Table 3 for this model are less than 0.05 (i.e. $\alpha = 0.05$, 95% confidence level) which indicates that the present quadratic model is statistically significant and shows that the agents have a substantial force on various responses. In conditions of code factors the terms in this case *A*, *B*, *C*, *D*, *BD*, *CD*, and A^2 are significant model terms. Values larger than 0.1000 indicate the model terms are not important. These insignificant model terms can be removed and test of lack of fit also displayed to be unimportant. The backward elimination is used to take out the insignificant terms from the quadratic model and shown in Table 4. The Model *F*-value of 447.34 implies the model is important. There is just a 0.01% chance that an *F*-value this large could occur due to interference. Values of "Prob > *F*" less than 0.0500 indicate model terms are significant. In this case *A*, B, *C*, *D*, *AD*, *BD*, *CD*, A^2, D^2 are significant model terms. Values greater than 0.1000 indicate the model terms are not significant. The "Pred R-Squared" of 0.9867 is in reasonable agreement with the "Adj R-Squared" of 0.9935; i.e. the difference is less than

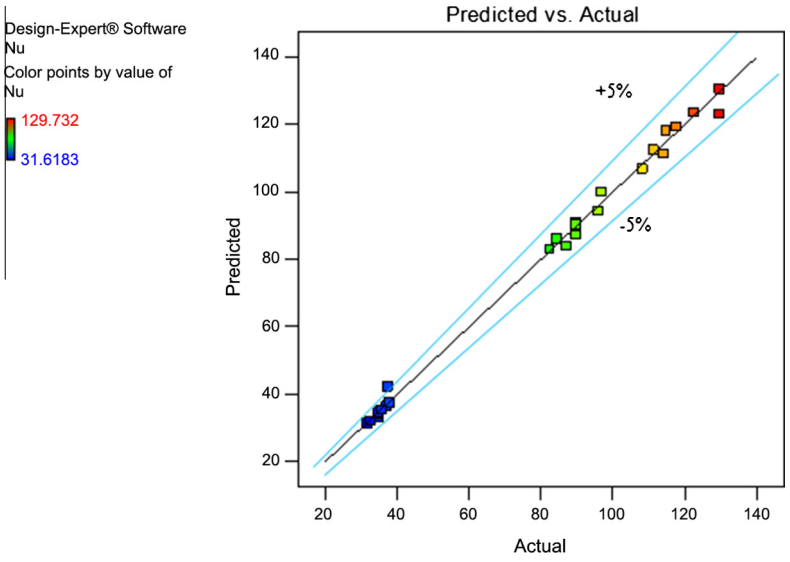

Figure 5a Comparison of experimental and predicted values of RSM model for Nusselt number.

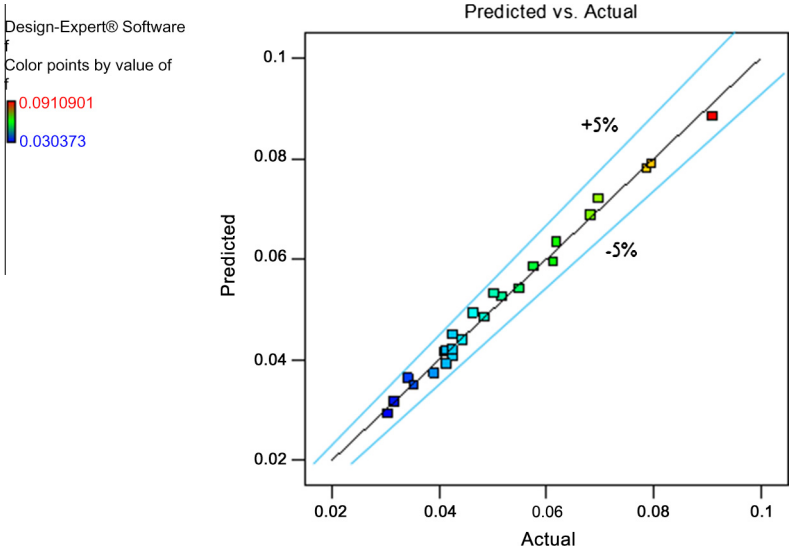

Figure 5b Comparison of experimental and predicted values of RSM model for friction factor.

0.2. "Adeq Precision" measures the signal to noise ratio. A ratio greater than 4 is desirable. In the present case ratio of 61.643 indicates an adequate signal. This model can be used to navigate the design space. A similar attempt is made to represent the effect of factors on the other response i.e. friction factor. The F test for friction factor is given in Table 5. The Model F-value of 148.43 implies the model is significant. There is only a 0.01% chance that an F-value this large could occur due to noise. Values of "Prob > F" less than 0.0500 indicate model terms are significant. In this case A, B, C, D, BD, A^2, B^2 are significant model terms. Values greater than 0.1000 indicate the model terms are not significant. The backward elimination is used to take out the insignificant terms from the quadratic model and shown in Table 6. In the backward elimination model the F-value of 195.13 implies the model is significant. There is only a 0.01% chance that an F-value this large could occur due to noise. Values of "Prob > F" less than 0.0500 indicate model terms are significant. In this case A, B, C, D, BD, A^2, B^2, D^2 are significant model terms. Values greater than 0.1000 indicate the model terms are not significant. The "Pred R-Squared" of 0.9714 is in reasonable agreement with the "Adj R-Squared" of 0.9853; i.e. the difference is less than 0.2. "Adeq Precision" measures the signal to noise ratio. A ratio greater than 4 is desirable. The ratio of 53.692 indicates an adequate signal and the model can be used to navigate the design space.

Through backward elimination process the final quadratic equation of response i.e. Nu and f in terms of coded and actual factors is presented as follows:

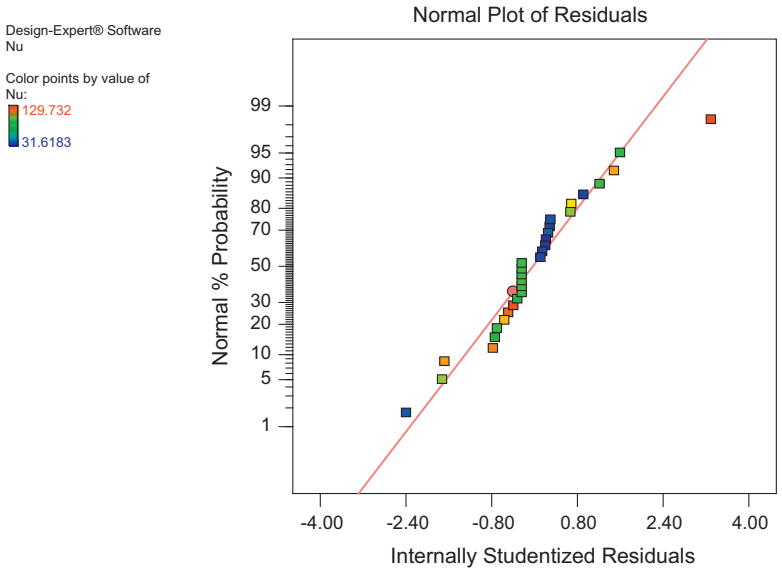

Figure 6a Normal probability plot residuals for the Nusselt number.

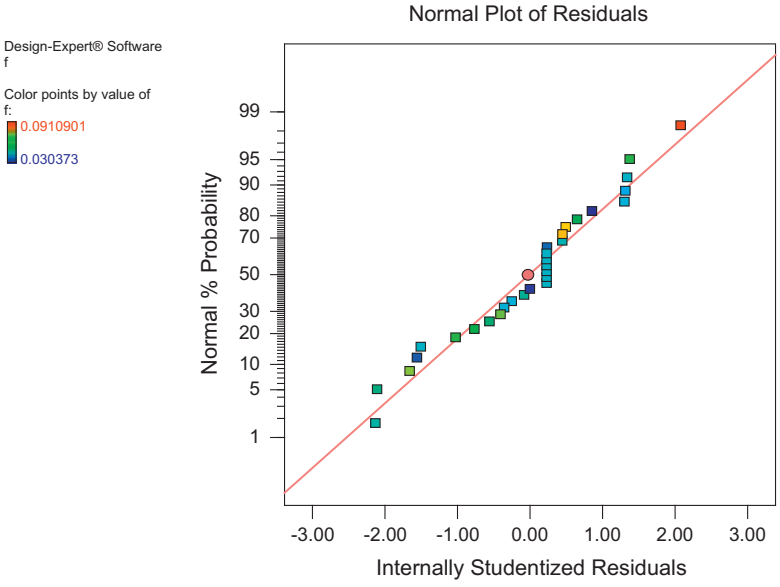

Figure 6b Normal probability plot residuals for the friction factor.

Final equation in terms of coded factors is

$$\begin{aligned}\mathrm{Nu} = {} & +86.36 + 1.95 \times A + 3.92 \times B - 3.31 \times C + 40.46 \times D \\ & + 1.49 \times AD + 2.27 \times BD - 2.30 \times CD - 5.12 \times A^2 \\ & - 2.74 \times C^2 - 3.72 \times D^2 \end{aligned} \quad (4)$$

Final equation in terms of coded factors is

$$\begin{aligned} f = {} & +0.043 - 4.323 \times 10^{-3} \times A + 0.014 \times B \\ & - 2.915 \times 10^{-3} \times C - 7.946 \times 10^{-3} \times D \\ & + 8.031 \times 10^{-4} \times AC - 9.201 \times 10^{-4} \times BC \\ & - 1.832 \times 10^{-3} \times BD + 2.89 \times 10^{-3} \times A^2 \\ & + 7.157 \times 10^{-3} \times B^2 + 2.433 \times 10^{-3} \times D^2 \end{aligned} \quad (5)$$

Final equation in terms of actual factors is

$$\begin{aligned}\mathrm{Nu} = {} & -18.77622 + 20.10299 \times (P/e) + 3.1003 \times (e/H) \\ & + 0.93628 \times \beta + 6.36237 \times 10^{-3} \times \mathrm{Re} \\ & + 2.06894 \times 10^{-4} \times (P/e) \times \mathrm{Re} + 2.75813 \times 10^{-3} \\ & \times (e/H) \times \mathrm{Re} - 2.65685 \times \beta \times \mathrm{Re} - 5.12332 \times (P/e)^2 \\ & - 0.019005 \times \beta^2 - 7.17235 \times 10^{-8} \times \mathrm{Re}^2 \end{aligned} \quad (6)$$

Final equation in terms of actual factors is

$$\begin{aligned} f = {} & +0.11101 - 0.017487 \times (P/e) - 0.26952 \times (e/H) \\ & - 1.09271 \times 10^{-4} \times \beta - 1.27663 \times 10^{-6} \times \mathrm{Re} + 6.69273 \\ & \times 10^{-5} \times (P/e) \times \beta - 6.69668 \times 10^{-4} \times (e/H) \times \beta \\ & - 2.22186 \times 10^{-6} \times (e/H) \times \mathrm{Re} + 2.8896 \times 10^{-3} \times (P/e)^2 \\ & + 0.54592 \times (e/H)^2 + 4.69325 \times 10^{-11} \times \mathrm{Re}^2 \end{aligned} \quad (7)$$

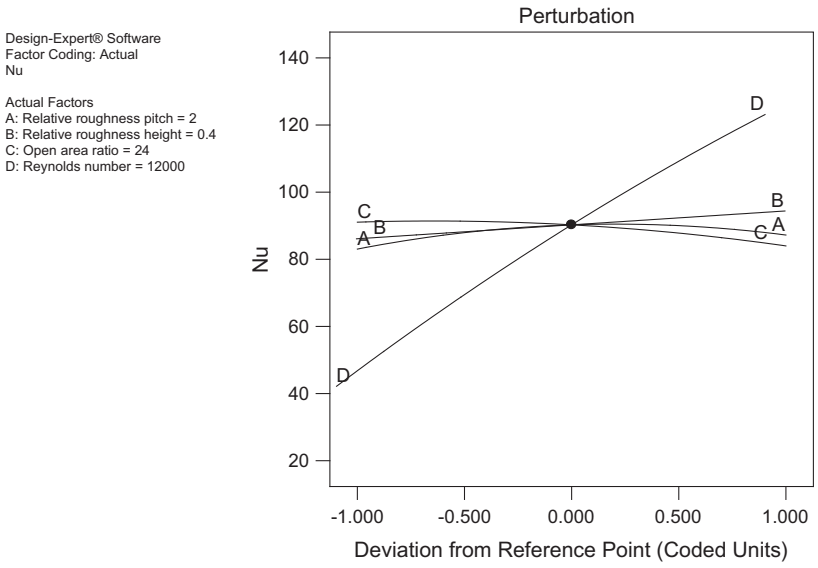

Figure 7 Variation of Nusselt number with (A) relative roughness pitch, (B) relative roughness height, (C) open area ratio and (D) Reynolds number.

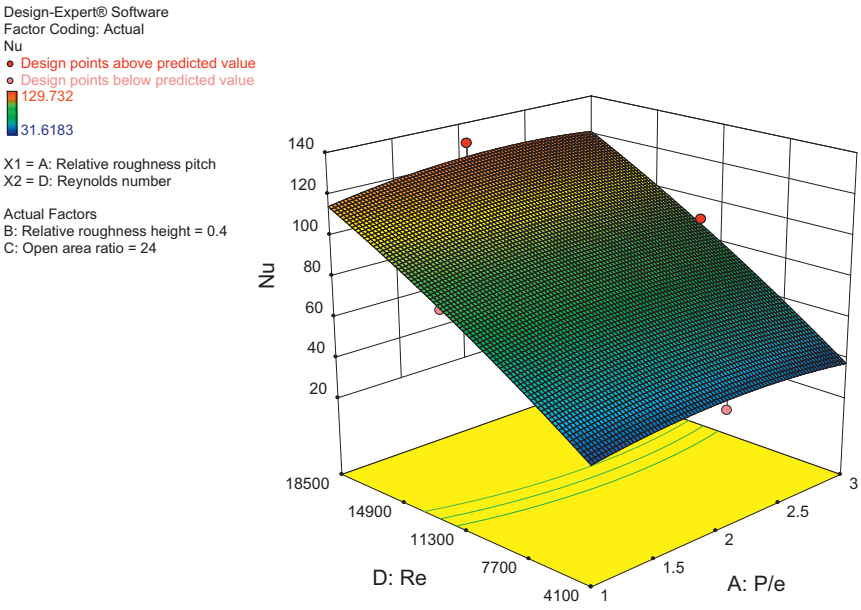

Figure 8 Effect of Reynolds number and relative roughness pitch on Nusselt number.

These above equations can be applied to predict the Nusselt number and friction factor of a V down perforated baffle roughened rectangular duct in the limited range of the geometrical and flow parameters with reasonably good accuracy.

Figs. 5a and 5b show the comparison of predicted values of the Nusselt number and friction factor with that of experimental values. The experimental and predicted values are in good understanding with each other, which assures the correctness of the information generated. The normal probability graph of residuals is also plotted for Nusselt number and friction factor and shown in Figs. 6a and 6b. It is seen that the residuals are falling in a straight line, which indicates that the errors are normally distributed.

Hence the model formed by RSM can be applied to predict the Nusselt number and friction factor of the V down perforated baffled roughened channel within the defined range of flow and geometrical parameters.

6.2. Effect of flow Reynolds number, relative roughness pitch, relative roughness height and open area ratio on Nusselt number

The effect of Reynolds number, relative roughness pitch, relative roughness height and open area ratio on the Nusselt number of V down perforated baffle roughened channel is presented in Figs. 7–10. It is seen from Fig. 7 that, with the

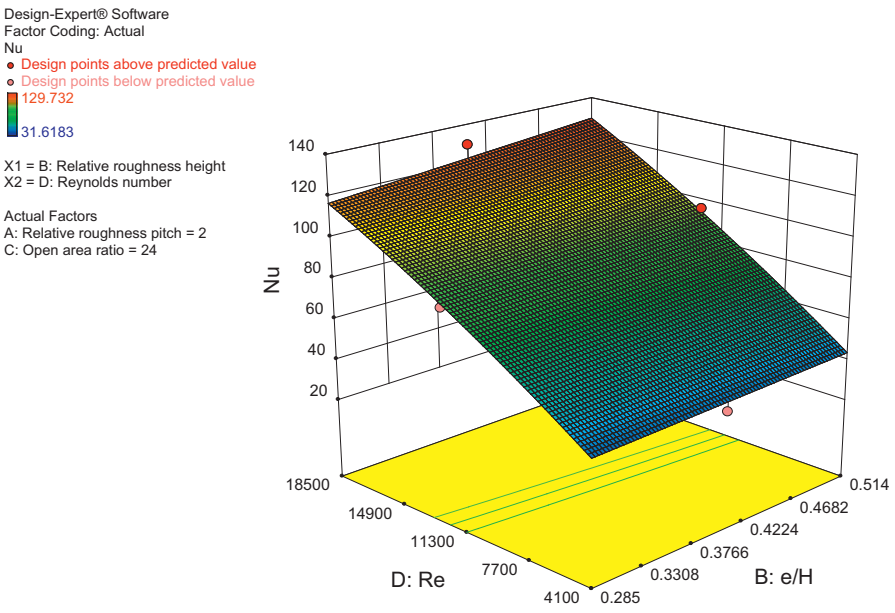

Figure 9 Effect of Reynolds number and relative roughness height on Nusselt number.

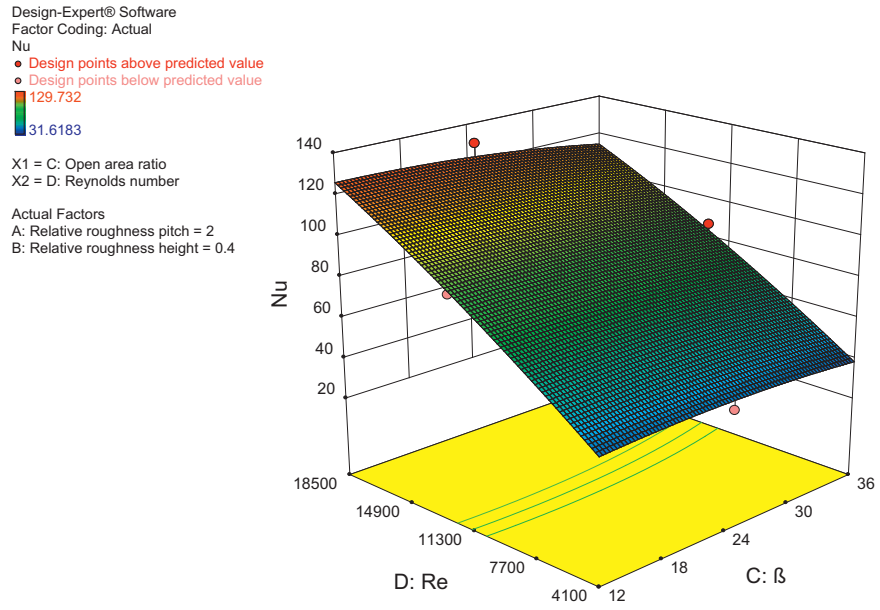

Figure 10 Effect of Reynolds number and open area ratio on Nusselt number.

increase in Reynolds number the Nusselt number increases, as with increase in flow Reynolds number the turbulent intensity increases which contributes to high heat transfer rate. The relative roughness pitch of 2 shows higher Nusselt number values, and this is ascribable to the flow reattachment and jet impingement without inference between jets leads to higher heat transfer rate. The same effect for Reynolds number and relative roughness pitch can be observed in Fig. 8. Figs. 9 and 10 show the effect of relative roughness height and open area ratio on Nusselt number and it is observed that the Nusselt number increases with increase in relative roughness height up to the value of 0.4, as to increase with relative roughness height of the strong vortex generated just downstream side and relatively proper mixing was also observed between the mainstream flow over the baffles and jet impinged flow. On increasing the value beyond 0.4 the decrement in heat transfer is observed, and this is ascribable to the establishment of strong vortex just downstream and provides more obstruction for the mainstream flow. The Nusselt number increases with gain in open area ratio option value of 24% and then starts decreasing, with gain in open area ratio beyond 24%; the jets spread immediately without impinging on the heated surface and it is also associated with inference among jets, which contributes to decreased lower rate of heat transport. The maximum value of the Nusselt number is observed to be 129.7 for relative roughness pitch of 2, relative roughness

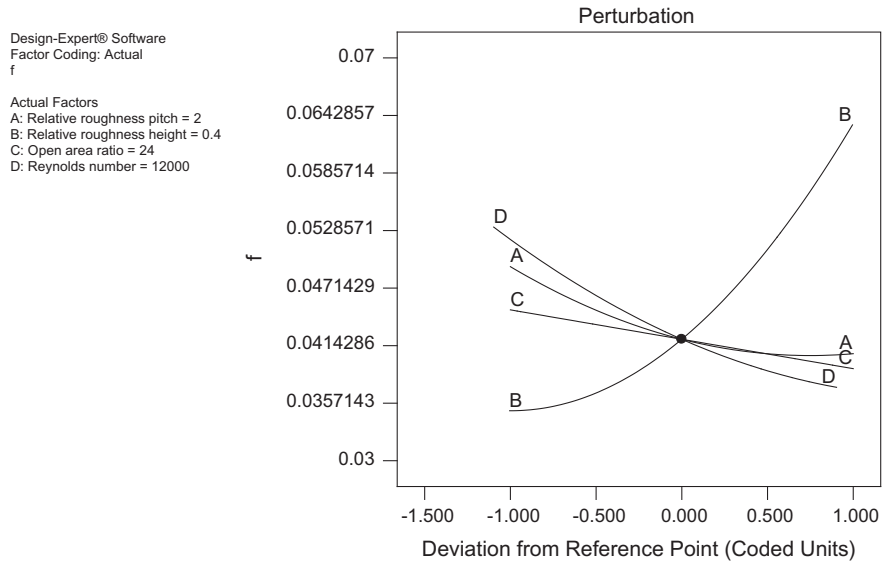

Figure 11 Variation of friction factor with (A) relative roughness pitch, (B) relative roughness height, (C) open area ratio and (D) Reynolds number.

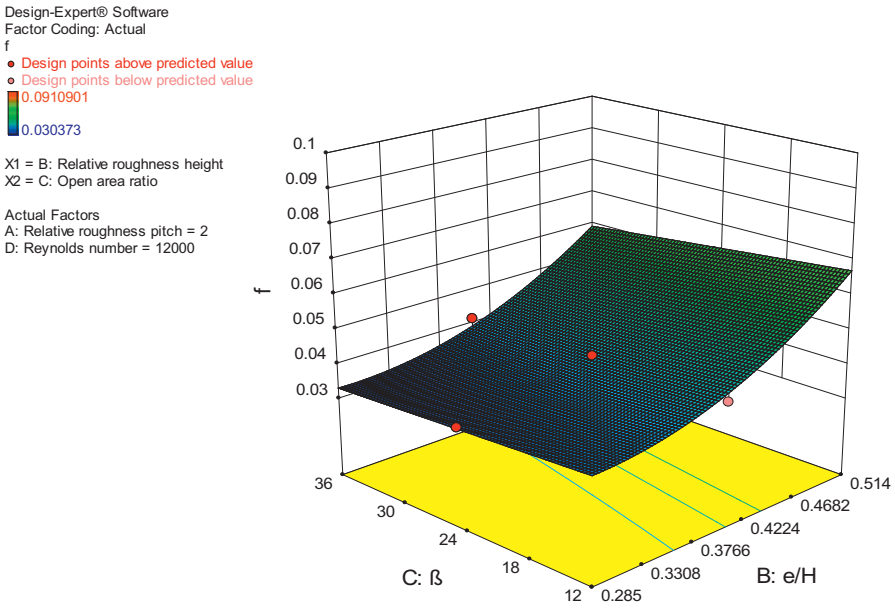

Figure 12 Effect of open area ratio and relative roughness height on friction factor.

height of 0.4, open area ratio of 24% and Reynolds number of 18,500, respectively.

6.3. Effect of flow Reynolds number, relative roughness pitch, relative roughness height and open area ratio on friction factor

The effect of Reynolds number, relative roughness pitch, relative roughness height and open area ratio is shown in Figs. 11–13. It is observed that with increase in open area ratio the friction factor decreases, as on increasing it the flow obstruction is reduced which leads less pressure drop penalty. The friction factor increases with increase in relative roughness height values, and this is due to the reason that on increasing the relative roughness height the flow blockage increases and more power is required to propel the fluid, which leads to higher friction factor values. The same effect of friction factor is observed in Fig. 13. The minimum value of friction factor of the order of 0.0303 is observed for the relative roughness pitch of 3, relative roughness height of 0.285, open area ratio of 24% and the flow Reynolds number of 18,500.

6.4. Optimization of designing parameters

The objective of the optimization for V down perforated baffle roughened rectangular channel is to provide the optimum roughness and flow parameters that give the upper limit value

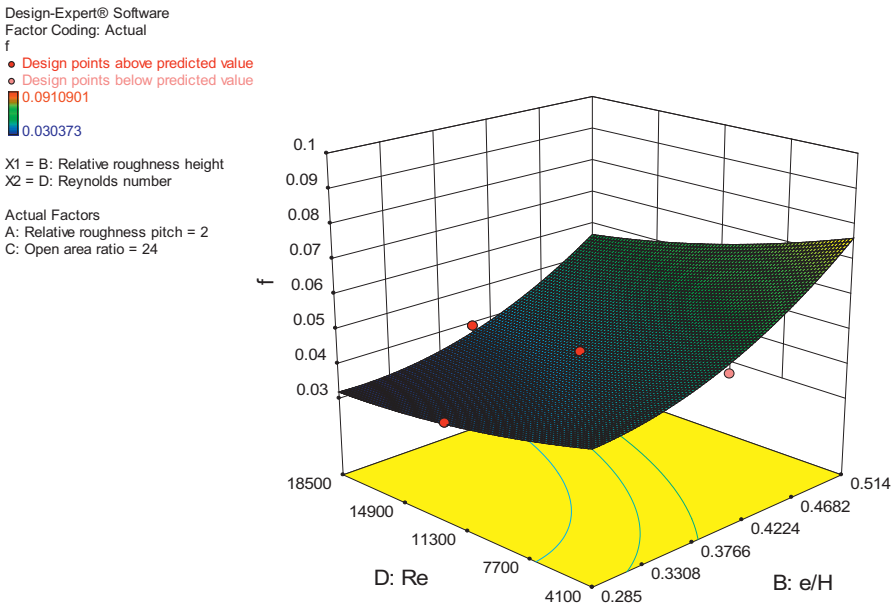

Figure 13 Effect of Reynolds number and relative roughness height on friction factor.

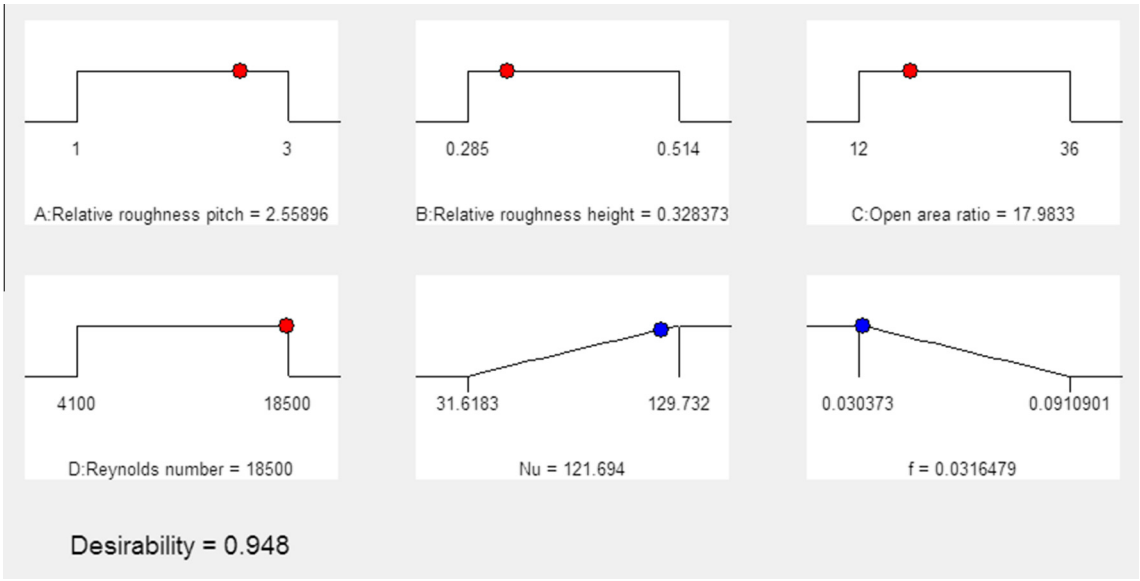

Figure 14 Ramp function graph of desirability for V down perforated baffle roughened rectangular channel.

of the Nusselt number at the monetary value of minimum pressure drop penalty. The combination of operating and flow parameters was selected based on the desirability values. The desirability values close to 1 unit were selected as the most effective parameters value with respect to the heat transfer and friction factor. The ramp functions and the desirability bar graphs are shown in Figs. 14 and 15, respectively. The optimal solution for the Nusselt number and friction factor for v down perforated baffle roughened rectangular channel is shown in Fig. 14. The range of input parameters and the associated responses range are given in Table 7. It is seen from Fig. 14 that the optimal values of input parameters are relative roughness pitch of 2.6, relative roughness height of 0.33, open area ratio of 18% and the flow Reynolds number of 18,500. The associated optimal values of responses for desirability closest to unity are given in Table 8. It is reported from Figs. 14 and 15 that approximately 100% of desirability is achieved for the output responses. Bar graph shows the overall desirability function of the responses. Desirability varies from 0 to 1 depending upon the nearness of the response toward the objective. The bar graph depicts how well each variable satisfies the criterion, a value close to one is considered proficient.

6.5. *Confirmation of experiments and RSM model*

To verify the data collected from the experiments for Nusselt number and friction factor from the quadratic model, a

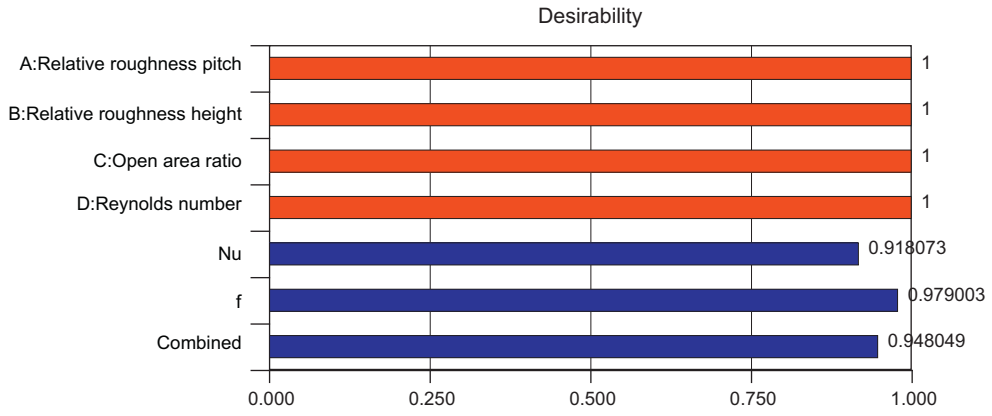

Figure 15 Desirability bar graphs for V down perforated baffle roughened rectangular channel.

Table 7 Range of input parameters and responses for optimization.

Parameter	Objective	Lower limit	Upper limit
Relative roughness pitch	Within range	1	3
Relative roughness height	Within range	0.28	0.51
Open area ratio	Within range	12	36
Reynolds number	Within range	4100	18500
Nusselt number	Maximum	31.61	129.73
Friction factor	Minimum	0.0303	0.091

Table 8 Optimum values of input parameters and responses.

Parameter	Objective	Optimum values
Relative roughness pitch	Within range	2.6
Relative roughness height	Within range	0.33
Open area ratio	Within range	18
Reynolds number	Within range	18,500
Nusselt number	Maximum	121.69
Friction factor	Minimum	0.031
Desirability		0.948

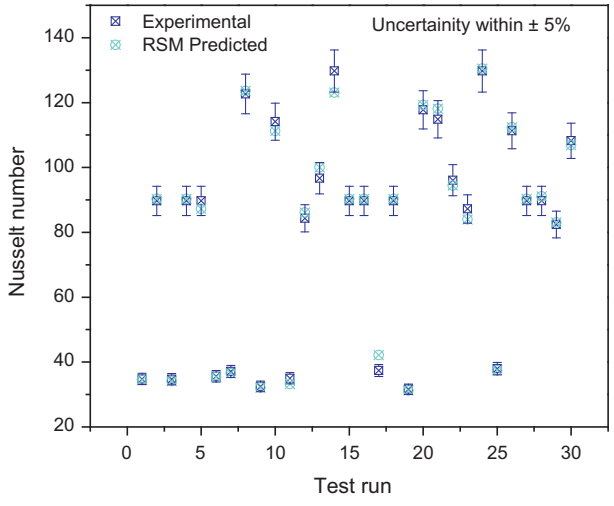

Figure 16 Shows the uncertainty, error bars for experimental and predicted (RSM) values of Nusselt number.

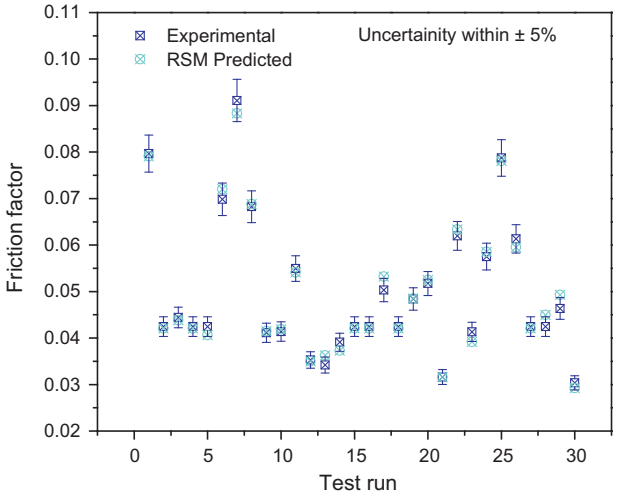

Figure 17 Shows the uncertainty, error bars for experimental and predicted (RSM) values of friction factor.

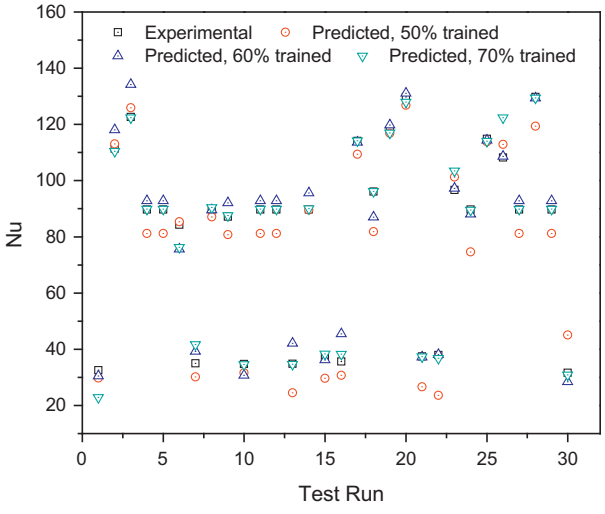

Figure 18 Comparison of Nusselt number for experiment and ANN for different trained data.

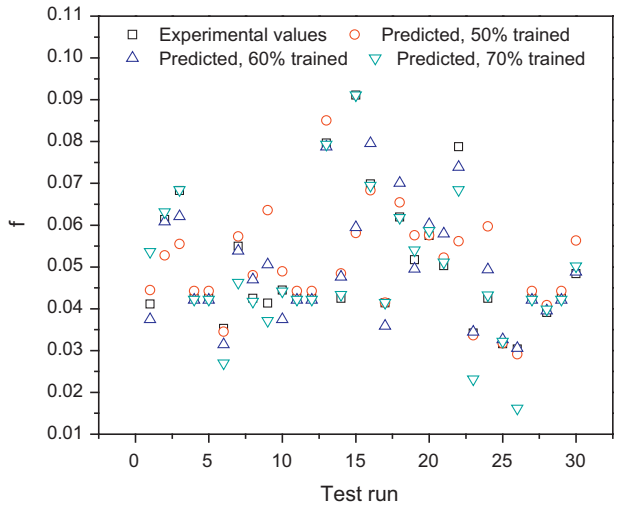

Figure 19 Comparison of friction factor for experiment and ANN for different trained data.

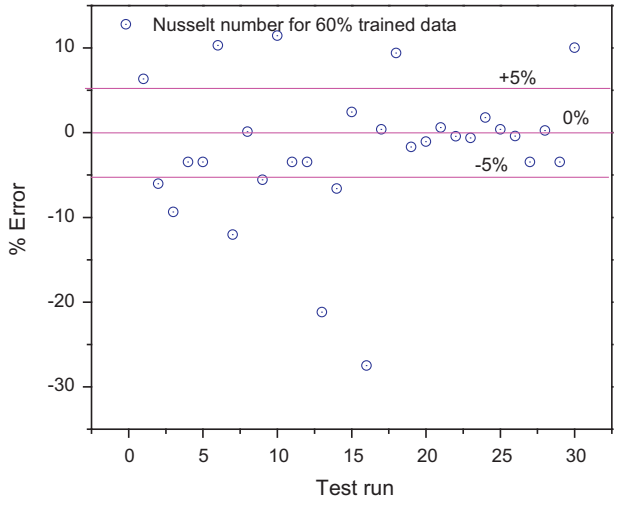

Figure 20 Shows the percentage error in predicted (ANN) and experimental values of Nusselt number.

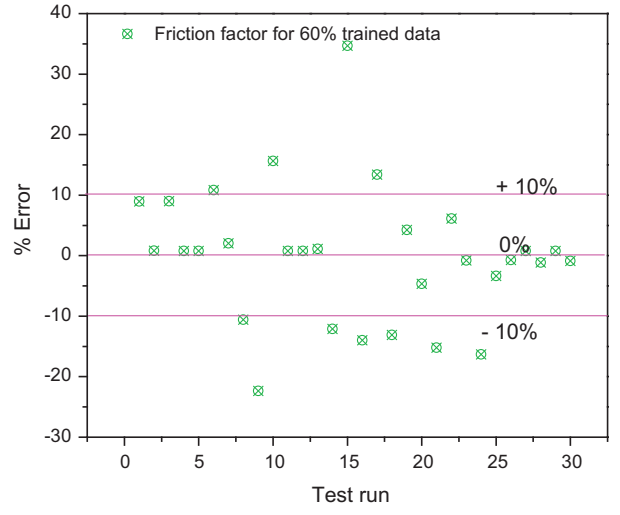

Figure 21 Shows the percentage error in predicted (ANN) and experimental values of friction factor.

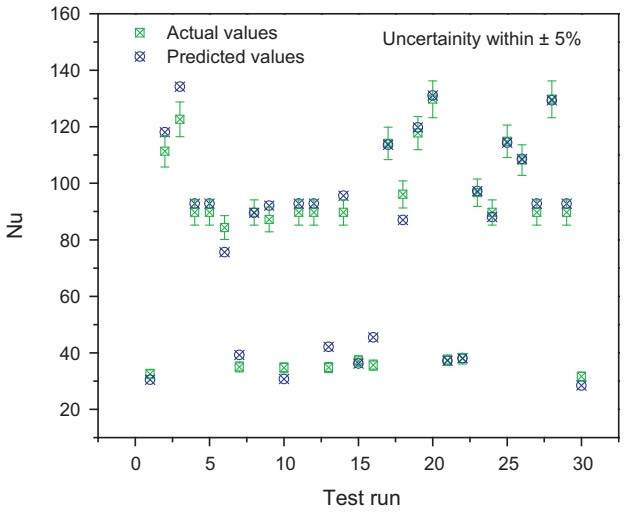

Figure 22 Shows the uncertainty error bars for experimental and predicted (ANN) values of Nusselt number.

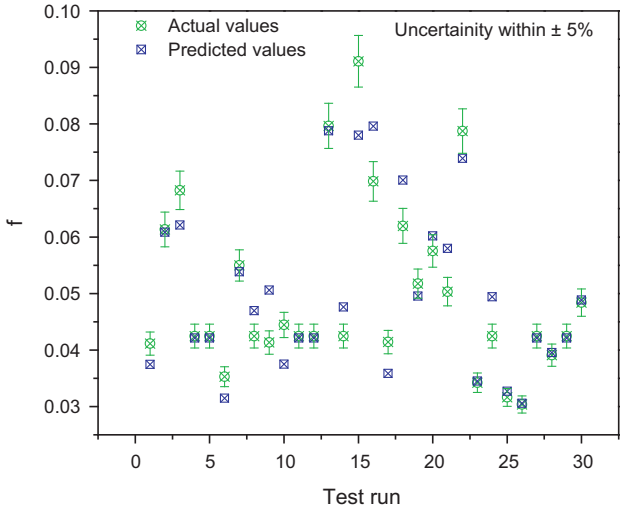

Figure 23 Shows the uncertainty error bars for experimental and predicted (ANN) values of friction factor.

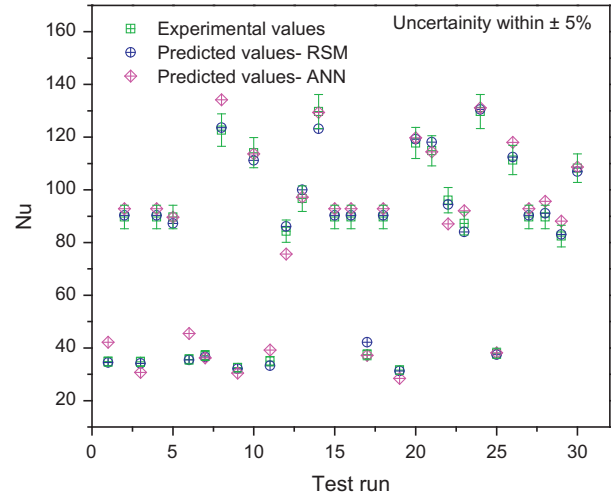

Figure 24 Shows the comparison of uncertainty error bars for experimental and predicted (RSM and ANN) values of Nusselt number.

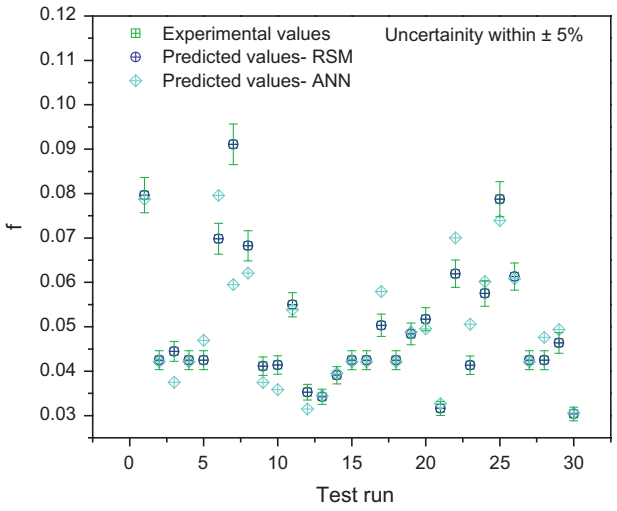

Figure 25 Shows the comparison of uncertainty error bars for experimental and predicted (RSM and ANN) values of friction factor.

comparison of the data values has been presented in Figs. 16 and 17, respectively. It is seen that all the predicted values by quadratic model are within ±5% error bars of the experimental values for both the responses i.e. Nusselt number and friction factor. All the experimental values for the each run are within the 95% prediction interval. Apparently, the quadratic model obtained is excellent accurate.

6.6. ANN based results

Feed-forward with backward propagation neural network 4-10-2 is used in the present investigation to train the experimental data given in Table 2. The total number of 30 runs of experiments was selected based on the RSM design for neural network training. The 50%, 60% and 70% of the total data were used for the training, while the rest is used for testing and validation. The variation in the data values for different percentages of trained data is presented in Figs. 18 and 19 for Nusselt number and friction factor, respectively. It has been observed that the 60% trained data values are close to the experimental data and thus the 60% training data are considered for the performance prediction of the V down perforated baffle roughened rectangular channel. The ANN predicted values for the 60% trained were compared with the experimental values and the error between the experimental and ANN predicted values was found in the range of ±10%. The error associated with the predicted and experimental values, along with each experimental run uncertainty for Nusselt number and friction factor is shown in respective Figs. 20–23.

Table 9 Comparison of the Nusselt number and friction factor values of experimental, RSM and ANN trained model.

	Input parameters				Response variables					
Test Run	P/e	e/H	β	Re	Nu_{Exp}	Nu_{RSM}	Nu_{ANN}	f_{Exp}	f_{RSM}	f_{ANN}
1	1	0.514	36	4100	34.78	34.49	42.15	0.0797	0.0791	0.0788
2	2	0.4	24	12,000	89.69	90.27	92.80	0.0425	0.0421	0.0421
3	3	0.285	12	4100	34.70	34.15	30.73	0.0444	0.0439	0.0375
4	2	0.4	24	12,000	89.69	90.27	92.80	0.0425	0.0421	0.0421
5	3	0.4	24	12,000	89.69	87.24	89.58	0.0425	0.0406	0.0470
6	3	0.514	36	4100	35.64	35.41	45.44	0.0698	0.0720	0.0796
7	1	0.514	12	4100	37.12	36.53	36.22	0.0911	0.0883	0.0595
8	1	0.514	12	18,500	122.67	123.61	134.16	0.0683	0.0688	0.0621
9	3	0.285	36	4100	32.51	32.11	30.45	0.0411	0.0415	0.0375
10	1	0.285	12	18,500	114.11	111.21	113.66	0.0414	0.0419	0.0359
11	1	0.285	12	4100	35.00	33.23	39.22	0.0550	0.0541	0.0539
12	2	0.285	24	12,000	84.32	86.11	75.63	0.0353	0.0350	0.0315
13	1	0.285	36	18,500	96.65	99.99	97.24	0.0342	0.0363	0.0345
14	2	0.4	24	18,500	129.73	123.13	129.39	0.0391	0.0373	0.0396
15	2	0.4	24	12,000	89.69	90.27	92.80	0.0425	0.0421	0.0421
16	2	0.4	24	12,000	89.69	90.27	92.80	0.0425	0.0421	0.0421
17	2	0.4	24	4100	37.40	42.19	37.17	0.0503	0.0532	0.0580
18	2	0.4	24	12,000	89.69	90.27	92.80	0.0425	0.0421	0.0421
19	1	0.285	36	4100	31.62	31.19	28.45	0.0484	0.0485	0.0488
20	3	0.514	36	18,500	117.77	119.26	119.75	0.0517	0.0525	0.0495
21	3	0.285	12	18,500	114.84	118.09	114.38	0.0316	0.0316	0.0327
22	2	0.514	24	12,000	96.06	94.40	87.04	0.0620	0.0634	0.0701
23	2	0.4	36	12,000	87.21	84.00	92.06	0.0413	0.0391	0.0506
24	3	0.514	12	18,500	129.73	130.48	131.11	0.0575	0.0585	0.0602
25	3	0.514	12	4100	37.95	37.45	38.11	0.0787	0.0781	0.0739
26	1	0.514	36	18,500	111.31	112.39	118.03	0.0613	0.0595	0.0608
27	2	0.4	24	12,000	89.69	90.27	92.80	0.0425	0.0421	0.0421
28	2	0.4	12	12,000	89.69	91.07	95.62	0.0425	0.0450	0.0476
29	1	0.4	24	12,000	82.43	83.06	88.09	0.0463	0.0493	0.0494
30	3	0.285	36	18,500	108.21	106.87	108.64	0.0303	0.0292	0.0306

6.7. Comparison of the RSM and ANN models

The RSM and ANN based predictive models for Nusselt number and friction factor were compared with the experimental values based on predictive errors. The values RSM and ANN are compared for 30 runs of experiments suggested in CCD design of RSM. The deviation in predictive values for Nusselt number and friction factor is more in the ANN predictive model than in the RSM design. The deviation of the values are represented in the form of the error bars of experimental values for each run and depicted in Figs. 24 and 25.

It is understood from Figs. 24 and 25 that all predicted values by RSM are within ±5% of the experimental values, as in the case of ANN model some of the values are deviated from the ±5% range of faults. The comparability of the values of the responses i.e. Nusselt number and friction factor based on the RSM quadratic model and the ANN trained model is presented in Table 9.

7. Conclusions

In this study, an effective procedure of response surface methodology (RSM) along with ANN has been applied for optimizing the thermal performance characteristics of the V down perforated baffle roughened rectangular channel. The relative roughness height, the relative roughness pitch, the open area ratio, and the flow Reynolds number are chosen as variables to analyze the thermal performance as responses in conditions of the Nusselt number and the friction component. The following conclusions are drawn from the study:

- The quadratic model generated by RSM design for Nusselt number and friction factor has been found suitable to predict the performance of the V down perforated baffle roughened rectangular channel. The deviation under the confidence level of 95% in the data values of experimentally collected and that generated from the RSM quadratic model assure the accuracy of the RSM model.
- The optimal values of input parameters are relative roughness pitch of 2.6, relative roughness height of 0.33, open area ratio of 18% and the flow Reynolds number of 18,500, with the desirability of the order of 0.95.
- The neural network is trained with various proportions of the total experimental data of RSM design and 60% training is found satisfactory, as the results of the ANN predicted model are in good agreement with the experimental results within uncertainty range of ±10%. It is concluded that the feed forward backward propagation 4-10-2 ANN is a most accurate architecture for prediction of turbulent heat transfer and flow resistance in V down perforated baffle roughened channel.
- The ANN predicted model values and RSM predicted values of Nusselt number and friction factor were also compared with the experimental values and it is found that the RSM quadratic model response values are in good agreement with the experimental values in the range of ±5% uncertainty. The RSM model found superior over the ANN model in the present study. It is thus concluded that both the ANN and RSM models can be used to predict the turbulent heat transfer and fluid flow characteristics of roughened rectangular channels.

References

[1] B. Lu, P.X. Jiang, Experimental and numerical investigation of convection heat transfer in a rectangular channel with angled ribs, Exp. Therm. Fluid Fluid Sci. 30 (2006) 513–521.

[2] R. Kamali, A.R. Binesh, The importance of rib shape effects on the local heat transfer and flow friction characteristics of square ducts with ribbed internal surfaces, Int. Commun. Heat Mass Transfer 35 (2008) 1032–1040.

[3] P. Promvonge, C. Thianpong, Thermal performance assessment of turbulent channel flows over different shaped ribs, Int. Commun. Heat Mass Transfer 35 (2008) 1327–1334.

[4] C. Thianpong, T. Chompookham, S. Skullong, P. Promvonge, Thermal characterization of turbulent flow in a channel with isosceles triangular ribs, Int. Commun. Heat Mass Transfer 36 (2009) 712–717.

[5] D.H. Lee, D.H. Rhee, K.M. Kim, H.H. Cho, H.K. Moon, Detailed measurement of heat/mass transfers with continuous and multiple V shaped ribs in rectangular channel, Energy 37 (2009) 1770–1778.

[6] P. Promvonge, Heat transfer and pressure drop in a channel with multiple 60 V baffles, Int. Commun. Heat Mass Transfer 37 (2010) 835–840.

[7] P. Promvonge, W. Changcharoen, S. Kwankaomeng, C. Thianpong, Numerical heat transfer study of turbulent square duct flow through inline V shaped discrete ribs, Int. Commun. Heat Mass Transfer 38 (2011) 1392–1399.

[8] G. Tanda, Effect of rib spacing on heat transfer and friction in a rectangular channel with 45 angled rib turbulators on one/two walls, Int. J. Heat Mass Transf. 54 (2011) 1081–1090.

[9] S. Singh, S. Chander, J.S. Saini, Heat transfer and friction factor correlations of solar air heater ducts artificially roughened with discrete V-down ribs, Energy 36 (2011) 5053–5064.

[10] P. Sriromreun, C. Thianpong, P. Promvonge, Experimental and numerical study on heat transfer enhancement in a channel with Z-shaped baffles, Int. Commun. Heat Mass Transfer 39 (2012) 945–952.

[11] P. Promvonge, W. Jedsadaratanachai, S. Kwankaomeng, C. Thianpong, 3D simulation of laminar flow and heat transfer in V-baffled square channel, Int. Commun. Heat Mass Transfer 39 (2012) 85–93.

[12] B.K.P. Ary, M.S. Lee, S.W. Ahn, D.H. Lee, The effect of the inclined perforated baffle on heat transfer and flow patterns in the channel, Int. Commun. Heat Mass Transfer 39 (2012) 1578–1583.

[13] S. Chamoli, N.S. Thakur, Heat transfer enhancement in solar air heater with V-shaped perforated baffles, J. Renew. Sustain. Energ. 5 (2013) 023122.

[14] S. Chamoli, N.S. Thakur, Correlations for solar air heater duct with V-shaped perforated baffles as roughness elements on absorber plate, Int. J. Sustain. Energ. (2013), http://dx.doi.org/10.1080/14786451.2013. 857318.

[15] S. Skullong, S. Kwankaomeng, C. Thianpong, P. Promvonge, Thermal performance of turbulent flow in a solar air heater channel with rib groove turbulators, Int. Commun. Heat Mass Transfer 50 (2014) 34–43.

[16] A.P. Singh, Varun Siddharta, Heat transfer and friction factor correlations for multiple arc shape roughness elements on the absorber plate used in solar air heaters, Exp. Thermal Fluid Sci. 54 (2014) 117–126.

[17] S. Caliskan, Experimental investigation of heat transfer in a channel with new winglet type vortex generators, Int. J. Heat Mass Transf. 78 (2014) 604–614.

[18] A. Bekele, M. Mishra, S. Dutta, Performance characteristics of solar air heater with surface mounted obstacles, Energy Convers. Manage. 85 (2014) 603–611.

[19] S. Skullong, P. Promvonge, Experimental investigation on turbulent convection in solar air heater channel fitted with

delta winglet vortex generators, Chin. J. Chem. Eng. 22 (2014) 1–10.
[20] S. Chamoli, N.S. Thakur, Thermal behavior in rectangular channel duct fitted with v-shaped perforated baffles, Heat Transfer Eng. 36 (5) (2015) 471–479.
[21] S. Chamoli, N.S. Thakur, J.S. Saini, A review on turbulence promoters used in solar thermal systems, Renew. Sustain. Energy Rev. 16 (5) (2012) 3154–3175.
[22] K.T. Chiang, F.P. Chang, Application of response surface methodology in the parametric optimization of a pin fin type heat sink, Int. Commun. Heat Mass Transfer 33 (2006) 836–845.
[23] K.T. Chiang, Modeling and optimization of designing parameters for a parallel plain fin heat sink with confined impinging jet using the response surface methodology, Appl. Therm. Eng. 27 (2007) 2473–2482.
[24] H. Han, B. Li, W. Shao, Multi objective optimization of outward convex corrugated tubes using response surface methodology, Appl. Therm. Eng. 70 (2014) 250–262.
[25] L. Sun, C.L. Zhang, Evaluation of elliptical finned tube heat exchanger performance using CFD and response surface methodology, Int. J. Therm. Sci. 75 (2014) 45–53.
[26] S. Karagoz, Investigation of thermal performance of S shaped enhancement elements by response surface methodology, Heat Mass Transf. (2014), http://dx.doi.org/10.1007/s00231-014-1413-2.
[27] S. Singh, P. Dhiman, Thermal and thermohydraulic performance evaluation of a novel type double pass packed bed solar air heater under external recycle using an analytical and RSM (response surface methodology) combined approach, Energy 72 (2014) 344–359.
[28] G.J. Zdaniuk, L.M. Chamra, D.K. Walters, Correlating heat transfer and friction in helically finned tubes using artificial neural network, Int. J. Heat Mass Transf. 50 (2007) 4713–4723.
[29] H. Esen, F. Ozgen, M. Esen, A. Sengur, Artificial neural network and wavelet neural network approaches for modelling of a solar air heater, Expert Syst. Appl. 36 (2009) 11240–11248.
[30] G. Xie, B. Sunden, Q. Wang, L. Tang, Performance predictions of laminar and turbulent heat transfer and fluid flow of heat exchangers having large tube-diameter and large tube-row by artificial neural networks, Int. J. Heat Mass Transf. 52 (2009) 2484–2497.
[31] I. Taymaz, Y. Islamoglu, Prediction of convection heat transfer in converging diverging tube for laminar air flowing using back-propagation neural network, Int. Commun. Heat Mass Transfer 36 (2009) 614–617.
[32] R. Beigzadeh, M. Rahimi, Prediction of heat transfer and flow characteristics in helically coiled tubes using artificial neural networks, Int. Commun. Heat Mass Transfer 39 (2012) 1279–1285.
[33] W. Yaïci, E. Entchev, Performance prediction of a solar thermal energy system using artificial neural networks, Appl. Therm. Eng. (2014), http://dx.doi.org/10.1016/j.applthermaleng.2014.07.040.
[34] S. Sreekanth, H.S. Ramaswamy, S.S. Sablani, S.O. Prasher, A neural network approach for evaluation of surface heat transfer coefficient, J. Food Process. Preserv. 23 (1999) 329–348.
[35] K. Levenberg, A method for the solution of certain problems in least squares, SIAM J. Numerical Anal. 16 (1944) 588–604.
[36] D. Marquardt, An algorithm for least-squares estimation of nonlinear parameters, SIAM J. Appl. Math. 11 (2) (1963) 431–441.
[37] M.T. Hagan, M. Menhaj, Training feed forward networks with the Marquardt algorithm, IEEE Trans. Neural Networks 5 (6) (1994) 989–993.